A Lumped Thermal Model Including Thermal Coupling and Thermal Boundary Conditions for High-Power IGBT Modules

Amir Sajjad Bahman, *Member, IEEE*, Ke Ma, *Member, IEEE*, and Frede Blaabjerg, *Fellow, IEEE*

***Abstract*—Detailed thermal dynamics of high-power IGBT modules are important information for the reliability analysis and thermal design of power electronic systems. However, the existing thermal models have their limits to correctly predict these complicated thermal behavior in the IGBTs: The typically used thermal model based on one-dimensional *RC* lumps have limits to provide temperature distributions inside the device; moreover, some variable factors in the real-field applications like the cooling and heating conditions of the converter cannot be adapted. On the other hand, the more advanced three-dimensional (3-D) thermal models based on finite-element method (FEM) need massive computations, which make the long-term thermal dynamics difficult to calculate. In this paper, a new lumped 3-D thermal model is proposed, which can be easily characterized from FEM simulations and can acquire the critical thermal distribution under long-term studies. Meanwhile, the boundary conditions for the thermal analysis are modeled and included, which can be adapted to different real-field applications of power electronic converters. Finally, the accuracy of the proposed thermal model is verified by FEM simulations and experimental results show a good agreement.**

***Index Terms*—Boundary conditions, finite-element method (FEM), insulated gate bipolar transistors (IGBTs), power converters, reliability, thermal modeling.**

I. Introduction

IN RECENT years, insulated gate bipolar transistor (IGBT) modules have been widely used in many industries, especially in high-power converter applications such as wind turbines, trains, and HVDC systems [1]. Due to cost concerns, industries are interested in higher power densities and integration of IGBT modules. However, in more integrated packages, the risk of failures in different parts of the IGBT module and the reliability of the power electronic systems become more critical. The reason originates from the increased heat generation in the semiconductors that makes the thermal management of the device more critical [2]. In order to implement the thermal management as well as the reliability assessment of the IGBT module, the first stage is to identify detailed temperatures in the critical locations accurately [3]. Temperature identification of IGBT modules is possible by different methods, e.g., thermography, thermocouples, thermosensitive electrical parameters, etc. However, applying these methods is coming with challenges such as cost, inaccuracy, inaccessibility, etc. Therefore, there is a trend in constructing of thermal models in the device, which represent the thermal system and give temperatures in desired locations. However, modeling the thermal system of high-power IGBT modules accurately is a challenging task, because several physical and operational factors influence the thermal behavior of the device. The physical factors are those ones related to geometries including the size and position of the semiconductor chips as well as temperature-dependent material properties in different layers of the IGBT module. One example of challenge is uneven temperature distribution among the chips and layers inside the IGBT module due to thermal couplings [4]. On the other hand, the operational factors include mission profiles and thermal dynamics that seriously affect the lifetime of the device. In a design for reliability (DfR) approach, mission profile−related temperature cycles in the critical locations like the junction and the solder are the important parameters to be identified [5].

Today, two groups of thermal models have been introduced. The first group of thermal models are built based on the one-dimensional lumped *RC* thermal network, e.g., Cauer or Foster thermal networks. These thermal models consist of an electrical circuit, including thermal resistance and thermal capacitance elements, to model the dynamics of the device temperature with respect to the power losses generated in the semiconductor chips [6]. Generally, these thermal models are given by the IGBT module manufacturer in the datasheets, and they are used for very fast and rough calculation of junction temperature. However, these one-dimensional thermal models cannot be used when considering three-dimensional (3-D) heat spreading in the thermal system.

The second group of thermal models includes those ones based on solving 3-D differential heat flow equation. In order

Manuscript received October 21, 2016; revised February 13, 2017; accepted March 29, 2017. Date of publication April 18, 2017; date of current version December 1, 2017. This work was supported by the Center of Reliable Power Electronics (CORPE), Department of Energy Technology, Aalborg University, Denmark. This paper was presented at the 2016 Applied Power Electronics Conference and Exposition (APEC), Long Beach, CA, USA, March 20–24, 2016. Recommended for publication by Associate Editor J. Rabkowski. *(Corresponding Author: Amir Sajjad Bahman.)*

A. S. Bahman and F. Blaabjerg are with the Department of Energy Technology, Aalborg University, Aalborg DK-9220, Denmark (e-mail: asb@et.aau.dk; fbl@et.aau.dk).

K. Ma is with the Department of Electrical Engineering, Shanghai Jiao Tong University, Shanghai 200240, China (e-mail: kema@sjtu.edu.cn).

Color versions of one or more of the figures in this paper are available online at http://ieeexplore.ieee.org.

Digital Object Identifier 10.1109/TPEL.2017.2694548

to solve such equations in a thermal system, different analytical methods like finite-element method (FEM), finite-volume method (FVM), or finite-difference method (FDM) have been widely used [7]–[9]. However, using these methods demand for large computational costs and these methods are not efficient to calculate the device temperature in long-term mission profiles.

On the other hand, mathematical solutions have been proposed, which constitute analytical expressions to generate compact 3-D thermal models, e.g., deconvolution solutions [10], Fourier series solutions [11], Green's function solutions [12], eigenvalue solutions [13], and the diffusive representation approach [14]. These solutions are based on analytical expressions, which are function of the design geometry and the material properties. Although these methods have the advantages of generality for the design of power module packaging, during the fast transient operations, they may lead to inaccuracy when considering the thermal coupling effects from the adjacent chips. Thermal coupling becomes critical, especially when the adjacent devices are of different kinds or they are loaded differently. For example, in [15], a photoelectrothermal model for LED systems has been proposed that comprises LED devices of different kinds and the coupling thermal resistances between LED devices have been accurately modeled. However, in the IGBT module, the thermal coupling for the critical layers is also needed to be modeled for accurate temperature estimation and reliability analysis in the long-term operation.

Apart from the internal parameters, the external conditions in the boundaries of the device, influence the thermal behavior of the IGBT modules. These conditions are needed to be considered in solving the 3-D heat differential equations [16]. In the IGBT module, the boundary conditions include the ambient temperature; the heat sources, i.e., power dissipation in the chips and the heatsink, i.e., cooling system. The effect of the boundary conditions on compact thermal models has been investigated in some research works. For example, in [12], a transient thermal model for multichip power modules has been introduced, which includes time-dependent boundary conditions. Similarly, in [17], a transient thermal model for data centers has been introduced, which includes modeling of server thermal mass changing with power dissipations and computer room air conditioning. It has been proven that the effect of the boundary conditions on the compact thermal models can be simplified into equivalent physical constraints to boundaries of the design geometry.

In a DfR approach of power electronics, it is important to model the thermal dynamics of the power semiconductors, including the IGBT modules with real-load profiles associated with the converter. For this reason, using a single platform with the same time constant for the circuit simulations and thermal modeling gives the advantages of fast calculation of critical temperatures in various load profiles.

This paper focuses on transformation of a simplified and accurate thermal model extracted from the FEM into the circuit simulator that considers all boundary conditions, thermal couplings, multilayer functions and gives temperatures with the high speed of the circuit simulator. In Section II, the modeling environment and fundamentals of the thermal network will be discussed and a generic 3-D thermal network will be introduced. In Section III, the concept of boundary conditions will be explained and the effect of boundary conditions in different layers of IGBT module will be investigated by means of FEM simulations. Section IV introduces the translation method of boundary conditions from FEM to a circuit simulator. According to the generic boundary-dependent RC elements, the 3-D thermal network becomes flexible to be used for different heat sources and heatsinks, and calculates temperatures in different locations and layers of the IGBT module in a relative fast and accurate way. In Section V, the introduced thermal model is verified by FEM simulations and also by experiments.

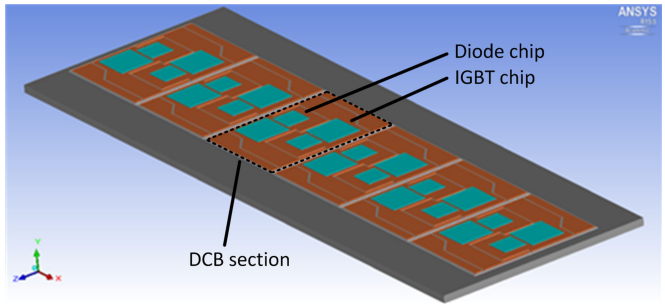

Fig. 1. Schematic of the high-power IGBT module modeled in ANSYS Icepak for FEM analysis.

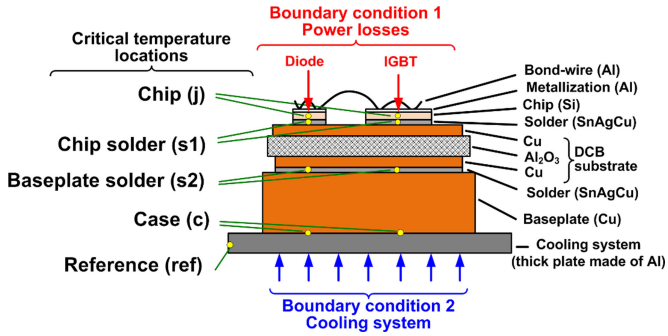

Fig. 2. IGBT module layers and boundary conditions.

II. Proposed 3-D Thermal Network

As shown in Fig. 1, a high-power IGBT module consisting of six direct-copper-bonded (DCB) sections in full-bridge topologies and connected in parallel is used as the case study. The materials of the IGBT module as well as boundary conditions for thermal analysis are shown in Fig. 2. In this study, boundary conditions mean the conditions that are existing or applied at all or a part of the boundary of the IGBT module externally, which influence the thermal behavior of the device and the thermal differential equations must be solved with respect to those conditions.

In this case study, there are two boundary conditions, one is in the chip as the heat source (power losses) and the other one is at the bottom of the baseplate as the cooling capability (heat sink/cooling system). The general thermal behavior of the IGBT module is explained by the heat equation, which means that the temperature of the IGBT module is a function of power loss

TABLE I
MATERIAL THERMAL PROPERTIES OF THE IGBT MODULE [17]

Material	Density $\mathrm{kg/m^3}$	Specific Heat $\mathrm{J/(kg \cdot K)}$	Conductivity $\mathrm{W/(m \cdot K)}$	
			Temp. (°C)	Conductivity
Silicon	2330	705	0.0	168
			100	112
			200	82
Copper	8954	384	0	401
			100	391
			200	389
Al_2O_3	3890	880	all	35
SnAgCu	7370	220	all	57

density q_{loss} [18]

$$\frac{\partial}{\partial t}T\left(x,t\right)-\alpha\Delta T\ \left(x,t\right)=\frac{q_{\mathrm{loss}}}{C_p\rho}\ ,\qquad \alpha\ =\frac{k_{th}}{C_p\rho} \tag{1}$$

where T is the temperature in each spot of design geometry and at a specific time, k_{th} is the thermal conductivity, C_p is the thermal capacitance, and ρ is the volumetric density of the material, where the spot is located. These important thermal characteristics for the materials used in the IGBT module under study are given in Table I.

It is noted that the conductivity of some materials is set to be temperature dependent according to [18]. Silicon and Copper show considerably lower thermal conductivity at higher temperatures, so these materials are more sensitive to boundary conditions. For simplicity, it is assumed that the IGBT module is adiabatic from the top and lateral surfaces, and therefore, all the generated heat is dissipated in the cooling system. In order to solve the heat equation [see (1)], the IGBT module geometry is modeled in the FEM simulation tool, *ANSYS Icepak* [19]. The FEM tool can divide the IGBT module geometry into much smaller volumes by a meshing process in order to make the heat equation solvable by the *ANSYS Icepak* numerical solver, *Fluent*.

When the geometry of the IGBT model is drawn and ready to be simulated by the FEM, some indexes should be introduced to analyze the impact of boundary conditions on thermal behavior of the IGBT module. Therefore, in this study, transient thermal impedance—that is the common parameter to describe the thermal behavior of an electronic system—is used. In a thermal system, the thermal impedance between two points in the transient operation $Z_{\mathrm{th}}(t)$ is explained as

$$Z_{th(a-b)}\ \left(t\right)=\frac{T_a\left(t\right)-T_b\left(t\right)}{P}\ =\frac{\Delta T_{ab}}{P} \tag{2}$$

where T_a and T_b are the temperatures in two nodes in the system and P is the total power dissipation, which is generated by the heat source. As a common practice, $T_b(t)$ is normally maintained to be a constant value rather than an instant variable for transient thermal characterization. So the thermal impedance is defined from junction to a fixed case temperature or to fixed ambient temperature. However, in the present study, the target is to derive partial transient thermal impedance curves between

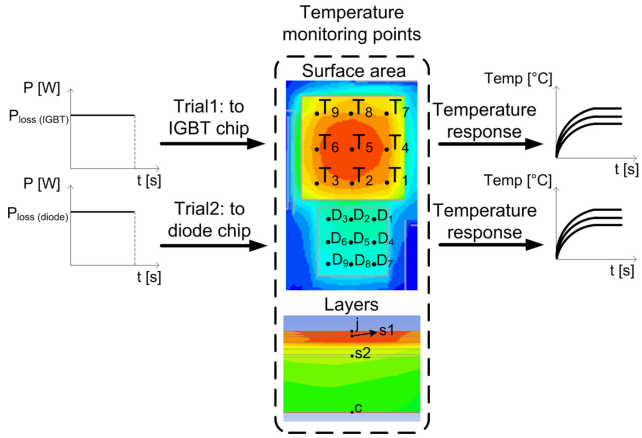

Fig. 3. Extraction process of nine branches of thermal networks from FEM.

the nodes. So, in transient operation, both $T_a(t)$ and $T_b(t)$ are the transient curves and the thermal impedance curves between layers will be extracted. To derive the thermal impedances, a single-step power loss with amplitude P_{loss} is injected to a heat source in the power module (IGBT chip or diode chip) until the junction temperature reaches the steady state. Then, by dividing the temperature difference between each two adjacent regions to power loss, a transient thermal impedance curve is obtained.

In order to extract the transient thermal impedance curves, step response analysis is implemented by FEM. When the curves are extracted, they will be fitted into a finite number of exponential equations described by

$$Z_{\mathrm{th}(a-b)}\ \left(t\right)=\sum_{i\ =\ 1}^{n}R_{\mathrm{th}_i}\ .\left(1-\exp\left(-\frac{t}{\tau_{\mathrm{th}_i}}\right)\right) \tag{3}$$

where R_{th_i} is the thermal resistance. τ_{th_i} is the time constant of the thermal system and equals to $R_{\mathrm{th}_i} * C_{\mathrm{th}_i}$ and n is the number of exponential terms to fit the $Z_{\mathrm{th}(a-b)}(t)$ well to the transient thermal impedance curve. Generally, four exponential terms are enough to fit the $Z_{\mathrm{th}(a-b)}(t)$ to the curve with minimum error. The number of exponential terms determines the number of *RC* elements in the *RC* thermal network [20].

As discussed earlier, the thermal impedances are defined between two nodes. In order to simplify the thermal model, critical nodes in the thermal system should be identified. The main catastrophic failures in the IGBT modules occur due to electrothermal stress in the bond-wires that lead to liftoff and aging of the solders that lead to cracks [21]. Therefore, the measurement nodes are defined in the surface of the chip, where the wires are bonded and solder layers. So, the IGBT module thermal system will be restructured vertically in four sections: junction to chip solder, chip solder to baseplate solder, baseplate solder to case, and case to reference, as shown in Fig. 2. The transient thermal impedances are extracted in the four sections. Besides, in order to monitor the temperatures in the heel of bond-wires, several temperature nodes will be defined horizontally in the IGBT module on the surface and in the other layers. Depending on the chip size and the number of bond-wires, the number of nodes can be different. In this case study, nine points have been selected to give enough information in the layers surface. The

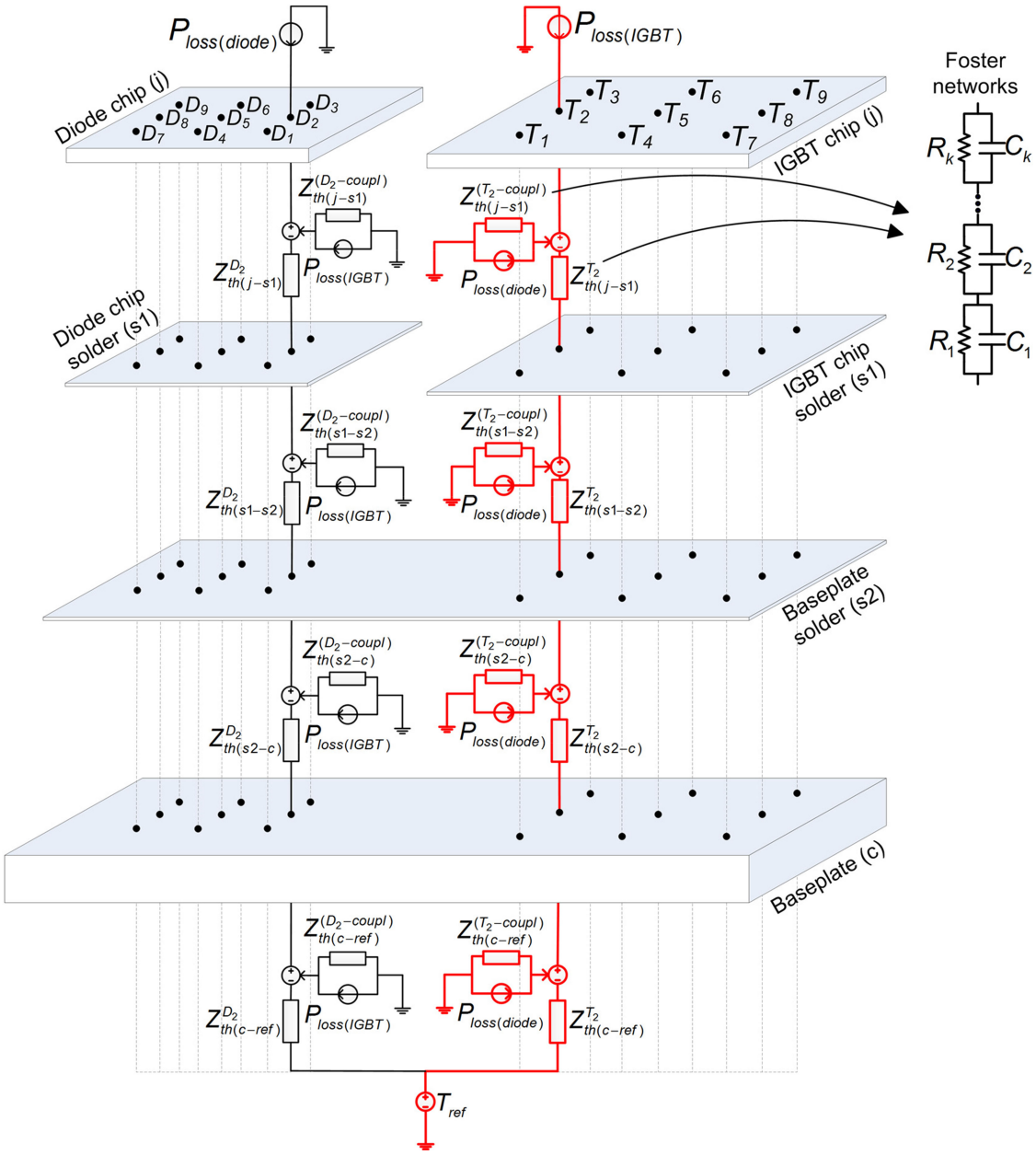

Fig. 4. 3-D thermal network from chip (junction) to reference (cooling temperature).

extraction process to derive the *RC* lumped elements is shown in Fig. 3.

Based on the described critical temperature locations, a 3-D thermal network is extracted, which includes all the mentioned nodes, different temperature locations on material layers, heat sources, heat sink, and thermal coupling effects from other heat sources. The schematic of the 3-D thermal network is shown in Fig. 4. In this thermal network, the thermal coupling from chips in neighbor DCB sections are not considered as the temperature variation among sections is more related to the overall cooling system which is not in focus here. Although significant differences have not been observed, more accurate models can be achieved by setting different boundary conditions of the model for different DCB sections.

The thermal network, which is used in this study is a Foster network and is widely used by industry due to the simplicity of extraction. The Foster model is conventionally utilized as a nonphysical model that can give temperature only in two ends of the network and the internal nodes between the *RC* components do not give physical meaning since they are not grounded. In the presented thermal model—as shown in Fig. 4—the Foster networks are built between several layers (chip, chip solder, baseplate solder, and baseplate) to extract temperatures in these layers. To extract the *RC* element values, the temperature of the higher critical layer and the lower critical layer are measured and the difference is divided to the power losses. Moreover, it is explained in [4] that the thermal coupling effects can also be modeled to thermal network. In the proposed thermal model,

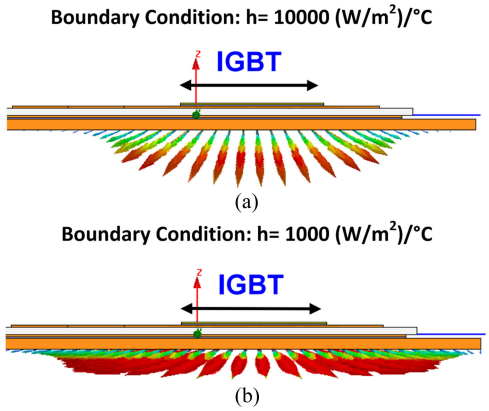

Fig. 5. Heat flux distribution in a power module for heat transfer coefficient of (a) 10 000 W/m^2·K and (b) 1000 W/m^2·K.

TABLE II
HEAT TRANSFER COEFFICIENTS FOR SOME COMMON FLUIDS (W/M^2·K) [18]

Free convection-air	5–25
Free convection-water	20–100
Forced convection−air	10–200
Forced convection−water	50–10 000
Boiling water	3000–100 000
Condensing water vapor	5000–10 000

thermal coupling effects among the points in the same chip have been removed for simplicity of the model. However, depending on the accuracy needed in the different dynamic operations of the IGBT module, the thermal coupling effects in the chip can be considered.

III. CHARACTERIZATION AND MODELING OF BOUNDARY CONDITIONS FOR THERMAL ANALYSIS

In order to understand the importance of the boundary condition effects in the thermal impedance of IGBT module, the cooling system variations and power loss variations are modeled by FEM simulations and the temperature responses are extracted in the corresponding points in the 3-D thermal network.

A. FEM Modeling With the Variation of Heatsink (Cooling System)

In this section, the thermal impedances for different cooling systems are analyzed including the fluid cooling system and the fixed case temperature. In all cases, a 50 W square pulse power is injected into the IGBT chip to fix the heat source boundary condition and the heatsinks are varied.

1) Heatsink With the Fluid Cooling System: To represent the capability of the fluid cooling system, different cooling mechanisms are considered in the heatsink. For each cooling mechanism, the equivalent heat transfer coefficient (htc) of the cooling system is extracted and modeled as a thick plate beneath the base plate of the IGBT module (as shown in Fig. 2). The parameter htc is defined to represent the amount of heat transferred between a solid and a fluid by convection [18] and is extracted by

$$\text{htc} = \frac{q}{\Delta T} \quad \left(\text{W/m}^2\text{K}\right) \tag{4}$$

where q is the heat that is transferred between solid and fluid (heat flux) and ΔT is the temperature difference between the solid surface and the fluid area. The heat flux q is defined as the thermal power $\dot{Q}$ – power losses in the IGBT module – per unit area

$$q = \frac{d\dot{Q}}{dA} \quad \left(\text{W/m}^2\right) \tag{5}$$

where A is the effective area for the heat dissipation of the heatsink. Moreover, the thermal resistance between the IGBT module and the heatsink R_{th} is defined based on the definition of htc

$$R_{\text{th}} = \frac{1}{\text{htc}.A} \quad (\text{K/W})\,. \tag{6}$$

As concluded from (6), a higher htc gives a smaller R_{th}. It means that with the higher heat convection between the IGBT module and the cooling system in a constant temperature rise, the heat flux will be more concentrated under the IGBT chips and the heat spreading will be decreased, as shown in Fig. 5. This phenomenon reduces the advantage of the big baseplate area in spreading the heat dissipation and the ΔT between the junction and the case will be increased. Depending on the cooling mechanism, htc varies from 10 W/m^2·K for natural convection systems to 10^5 W/m^2·K for phase change cooling systems. Some typical *htc*s used in the thermal systems are listed in the Table II.

As explained in Section II, transient thermal impedances are extracted for different *htc*s. In this paper, the *htc*s in the range of 3000 < htc <100 000 W/m^2·K are used that are reasonable values for the water cooling system of the IGBT module. According to these values, the transient thermal impedances, which are extracted by FEM, are shown in Fig. 6. It is clear that the most influenced layer in the thermal system is from the case to the reference (cooling fluid temperature) because this layer is the closest one to the heatsink and the heat removes the highest heat dissipation.

2) Heatsink With Fixed Case Temperature: On the other hand, the effect of fixed case temperature on the thermal impedance of the IGBT module is studied. To model the fixed case temperature, in the FEM environment, a thick plate is placed beneath the baseplate (see Fig. 2). There are two options to define the boundary conditions: 1) conductive heat transfer with a constant temperature, and 2) convective heat transfer with an equivalent heat transfer coefficient. As observed in the experiments, the case temperature is hardly constant even with

TABLE III
THERMAL IMPEDANCES IN DIFFERENT LAYERS BY CHANGING THE BOUNDARY CONDITIONS

Boundary Conditions	$Z_{\text{th}}j-s_1$ (%)	$Z_{\text{th}}s_1-s_2$ (%)	$Z_{\text{th}}s_2-C$ (%)	$Z_{\text{th}}C$-ref (%)
Cooling system	2.06	3.05	12.6	88
Fixed case temperature	42.62	0.47	1.32	0.6

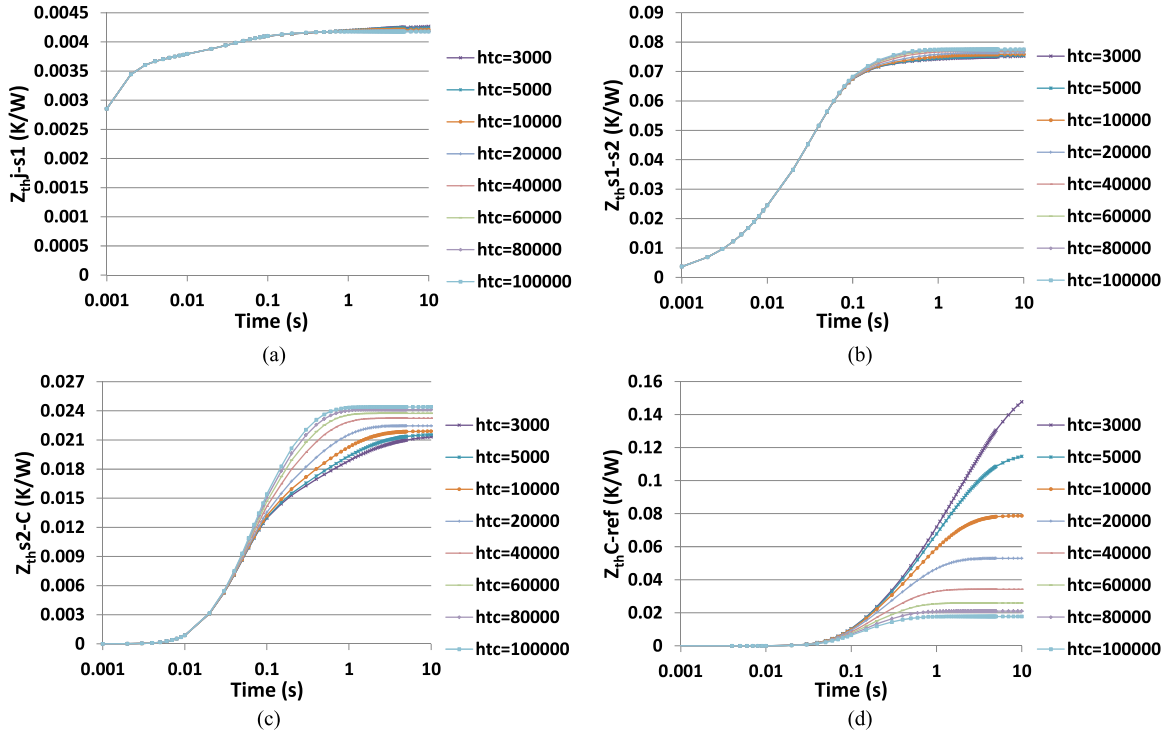

Fig. 6. Transient thermal impedances for different cooling systems (htc in W/m^2·K) in different layers of the T_2 branch (see Fig. 4): (a) junction to chip solder, (b) chip solder to baseplate solder, (c) baseplate solder to case, and (d) case to reference.

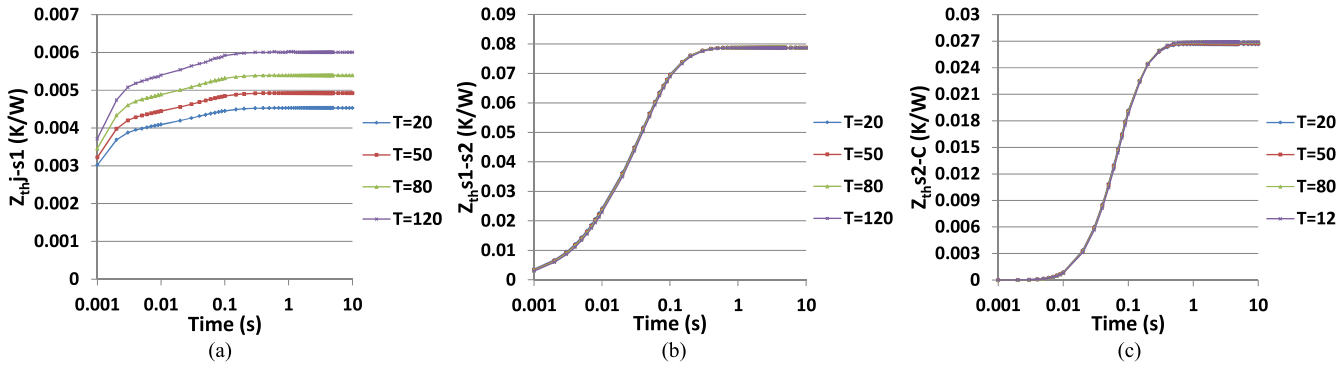

Fig. 7. Transient thermal impedances for different fixed case temperatures (T in °C) in different layers of the T_2 branch (see Fig. 4): (a) junction to chip solder, (b) chip solder to baseplate solder, and (c) baseplate solder to case.

a controlled cooling system as it cannot be maintained constant and it will increase slightly with a constant slope [20]. So, a heat transfer coefficient is selected as the boundary condition. As shown in (4) with a fixed value of heat flux (proportional to power losses) and very small values of ΔT (0.8 °C), the equivalent heat transfer coefficient will be very high (around 100 000 W/(m^2·K)). More discussions about the boundary conditions in the fixed case temperature are given in [20]. The reference temperature beneath the thick plate is fixed to a constant value and the heat transfer coefficient between the thick plate and the baseplate is set to 100 000 W/(m^2·K). In this study, the case temperature is varied in the range of 20–120 °C. The results are shown in Fig. 7. As it is seen, the most influenced section is the junction to chip solder. When the constant temperature is forced to the case, a temperature shock will be injected to the IGBT module. So, with different thermal properties of materials at different temperatures, the thermal impedance will be changed specially in the upper layers. So, the heat generated in the chip does not propagate to the lower layers and tends to be remained in the upper layers.

B. FEM Modeling With Variation of Heat Source (Power Losses)

To study the effect of heat sources on the thermal impedance of the IGBT module, the heat sink is fixed to htc, which is equal to 5000 W/m^2·K and the IGBT chip is excited with the different single-step power losses. The thermal impedance at

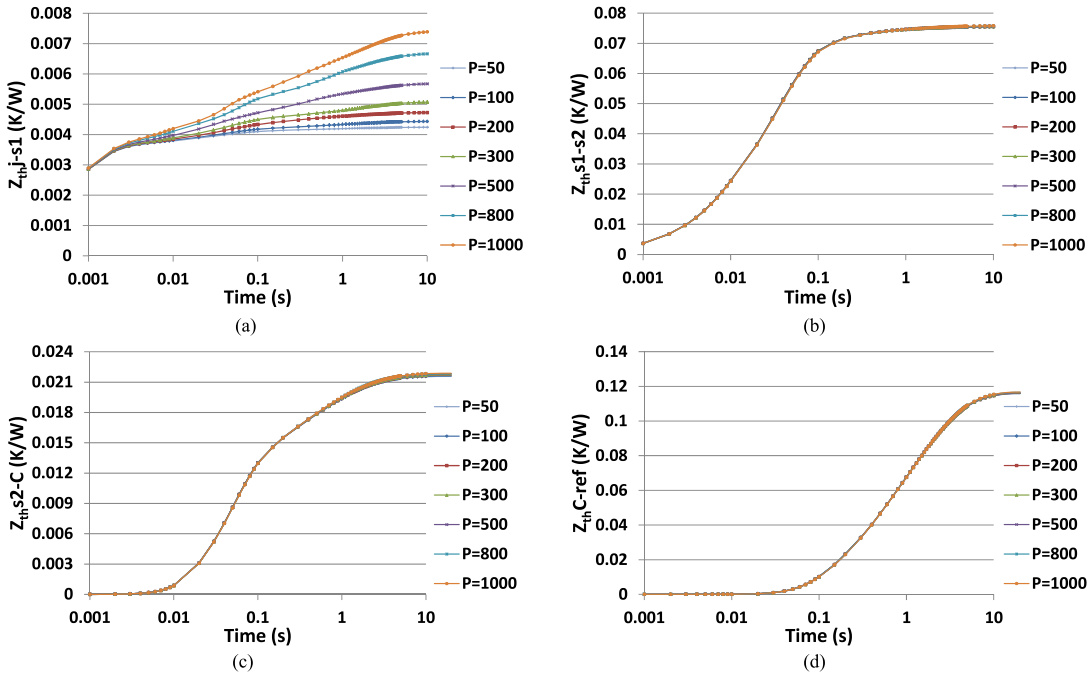

Fig. 8. Transient thermal impedances for different power losses (P in W) in different layers of the T_2 branch (see Fig. 4): (a) junction to chip solder, (b) chip solder to baseplate solder, and (c) baseplate solder to case, and (d) case to reference.

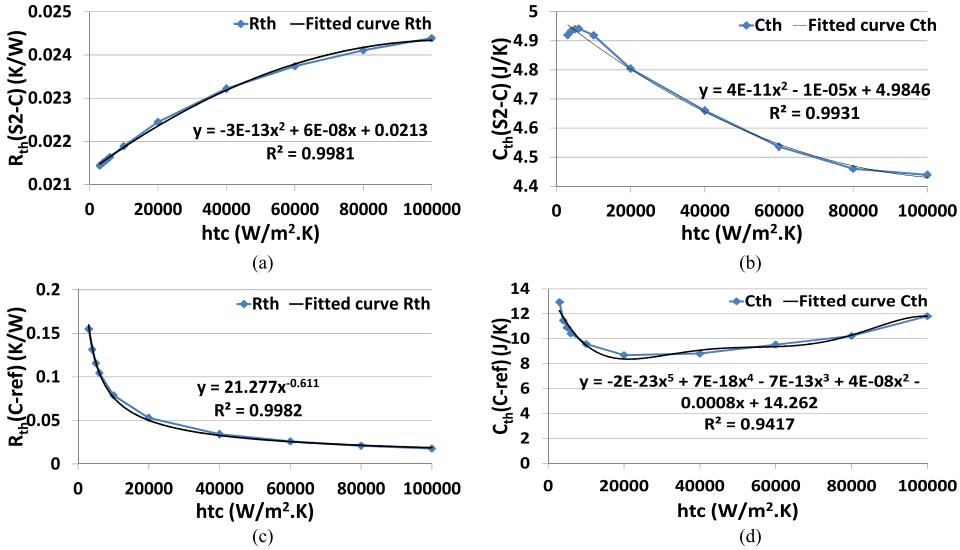

Fig. 9. Curve-fitted thermal resistance and thermal capacitance for different cooling systems ($R_{\rm th}$ is the thermal resistance and $C_{\rm th}$ is the thermal capacitance): (a) baseplate solder to case thermal resistance, (b) baseplate solder to case thermal capacitance, (c) case to reference thermal resistance, and (d) case to reference thermal capacitance.

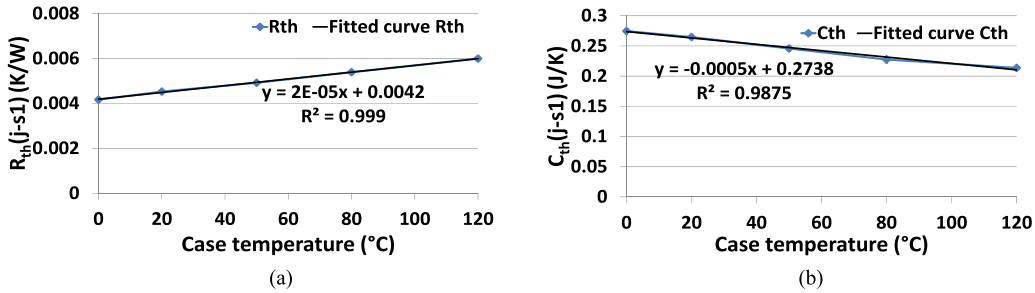

Fig. 10. Curve-fitted thermal resistance and thermal capacitance for different fixed case temperatures ($R_{\rm th}$ is the thermal resistance and $C_{\rm th}$ is the thermal capacitance): (a) junction to chip solder thermal resistance and (b) junction to chip solder thermal capacitance.

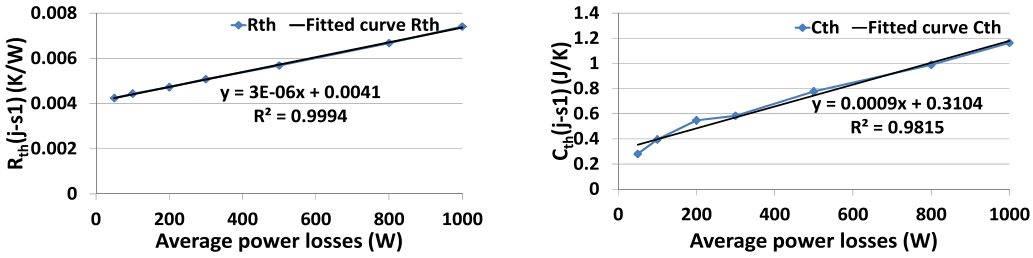

(a) (b)

Fig. 11. Curve-fitted thermal resistance and thermal capacitance for different power losses (R_{th} is the thermal resistance and C_{th} is the thermal capacitance): (a) junction to chip solder thermal resistance and (b) junction to chip solder thermal capacitance.

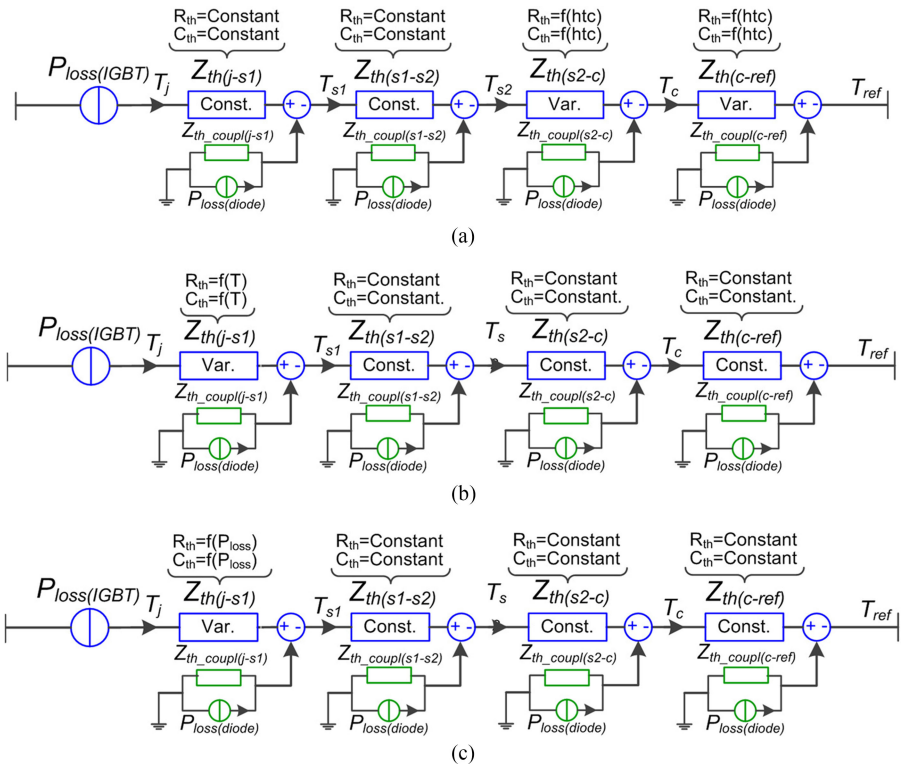

Fig. 12. Schematic of one branch of 3-D thermal network (highlighted in red in Fig. 4) with different boundary conditions: (a) variation of fluid cooling system, (b) variation of hotplate, and (c) variation of power losses.

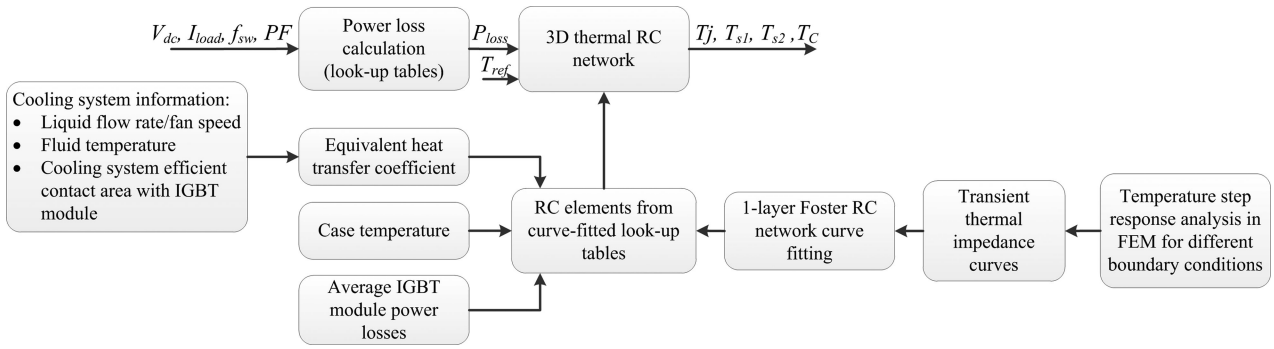

Fig. 13. Schematic of the proposed boundary-dependent thermal model for fast simulations.

different power losses are shown in Fig. 8. As it is seen, the most influenced thermal impedance is the section from the junction to the chip solder. This is a secondary effect of the fixed-case temperature, and similar variations of the thermal conductivity of the Silicon at different temperatures affect the junction to chip solder thermal impedance variation.

IV. Transformation of Boundary Conditions from FEM Model to Lumped *RC* Thermal Network

As discussed earlier, FEM is a time-consuming method demands for large computations, so it can be applied in the short-timescales. In longer load profiles, i.e., one-day to one-year mission profiles, the FEM simulation is not efficient. In order to overcome this problem, thermal models are needed that are accurate enough to give temperatures in critical locations and can be used for fast simulations of large data [22]. A solution is to model the thermal behavior of the IGBT modules in the fast circuit simulators with simple equivalent electrical elements. But currently it is difficult to include the effect of boundary conditions in the thermal models to be used in the circuit simulators. For this reason, simplified boundary-dependent thermal model should be translated from the FEM to the circuit simulator in order to instruct more generic, accurate, and fast thermal model. Therefore, it is proposed to apply step response analysis for different boundary conditions in FEM—at least for the limited number of conditions that the IGBT module is imposed to those conditions. By simulating the FEM models, transient thermal impedance curves are extracted and mathematically fitted to a 3-D network. As shown in Fig. 4, the partial Foster networks in the thermal model are flexible from one *RC* layer to multiple *RC* layers, depending on the optimum fitting. However, in order to simplify the process, one *RC* layer is used in this paper.

The *RC* elements in the regions, which are not varied by the boundary conditions, are shown as constant values. For better understanding of the idea, per-unit values of the thermal impedances in each layer are calculated by (7)

$$Z_{\mathrm{th}}\ (\%) = \frac{Z_{\mathrm{th}}\,(\max) - Z_{\mathrm{th}}\,(\min)}{Z_{\mathrm{th}}\,(\max)}\ \times 100 \qquad (7)$$

where $Z_{\mathrm{th}}(\%)$ is the per-unit value of the thermal impedance, $Z_{\mathrm{th}}(\max)$ and $Z_{\mathrm{th}}(\min)$ are, respectively, the maximum and minimum thermal impedances in the steady-state condition by varying the boundary conditions. The per-unit values are given in Table III. As it is seen for the values less than 5%, we assume the thermal impedance is not changing with the boundary conditions.

The *RC* element values in respect to the different cooling systems are shown in Fig. 9. For a higher accuracy of the thermal model, the thermal coupling branches are connected to the main branch as the controlled voltage sources. As described in Section II, the highly affected regions are from the baseplate solder to the case and from the case to the reference. The variation is mathematically curve fitted to determine the generic model for various cooling mechanisms. In the given curves, the horizontal axis shows different *htc*s (different cooling conditions) and the vertical axis shows the respected thermal resistance and thermal capacitance values. The curve-fitted linear mathematical model and respected *R*-squared values are also shown besides the curves.

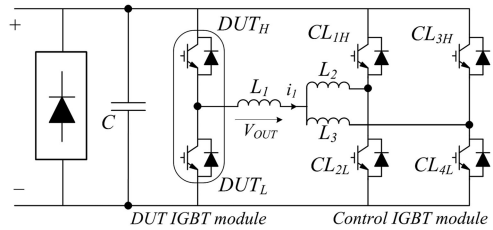

Fig. 14. Schematic of two-level voltage-source dc–ac converter (2L-VSC).

TABLE IV
Parameters of Converter Shown in Fig. 14

DC-bus voltage V_{dc}	690 V
Rated load current I_{load}	variable up to 900 A (peak)
Fundamental frequency f_o	6 Hz
Switching frequency f_{sw}	2.5 kHz
Filter inductor L_1	350 μH
IGBT module	1700 V/1000 A

For all cases, the *R*-squared values are at least 0.9 for a better accuracy of the curve fitting [23]. The generic thermal models for the variation of case temperatures and power losses are shown in Figs. 10 and 11. The schematic of one branch of the 3-D thermal network (highlighted in red in Fig. 4) with a variation of different boundary conditions are shown in Fig. 12. It should be mentioned that the identification of thermal coupling branches also follows the same methods as the main thermal branch.

By variation of the *RC* elements in the 3-D thermal network, a flexible thermal network is developed, in which the *RC* elements are dependent on the boundary conditions. In other words, by the presented approach, the thermal model of IGBT module can get feedback from the power losses and cooling system in transient operation and calculate accurately the temperatures in different locations with very high simulation speed. A schematic is shown in Fig. 13 to describe the transformation process of the boundary conditions from FEM to circuit 3-D thermal network.

V. Verifications

To validate the boundary dependent thermal models, first, the thermal network is established in a circuit simulator environment (e.g., PLECS) and the temperature responses are compared with FEM simulations (e.g., ANSYS Icepak) in three sample boundary conditions. In order to find the power loss profile, the IGBT module is loaded with a three-phase dc–ac two-level voltage-source converter (2L-VSC). The schematic of the converter is shown in Fig. 14, and the detailed converter specifications are listed in Table IV. The IGBT, diode, and other components are selected as typical values, which are used in the grid-side inverters for wind power applications.

First, the validity of one-layer *RC* Foster network compared to a four-layer *RC* network (see Fig. 4) is tested. The curve-fitting process is implemented for both cases and the extracted *RC* values are placed in the 3-D thermal network. The conditions

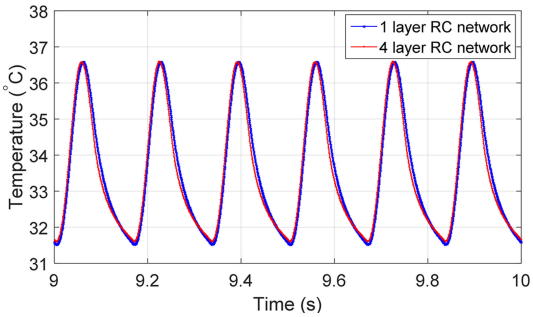

Fig. 15. Temperature results calculated by one-layer *RC* network comparing to four-layer *RC* network.

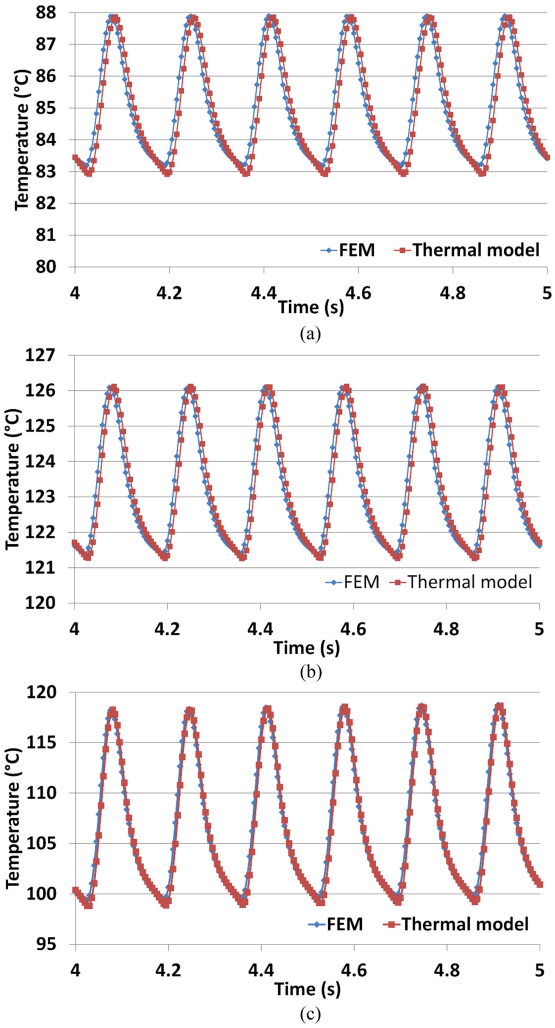

Fig. 16. Junction temperatures from simulated simplified thermal model and FEM simulation at different boundary conditions: (a) htc = 20 000 W/m^2·K, (b) T_C = 120 °C, and (c) P_{loss} = 100 W.

for the test are set as: I_{load} = 450 A(peak), T_{ref} = 30 °C, and htc = 5000 W/m^2·K. As it is shown in Fig. 15, one *RC* layer can estimate the junction temperature with high accuracy compared with the multilayer *RC* network. So, one-layer curve fitting can be used for the 3-D thermal network. The junction temperature results for a selected point on the IGBT chip (T_2 in Fig. 4) are shown for the cases of htc = 20 000 W/m^2·K, T_C = 120 °C, and

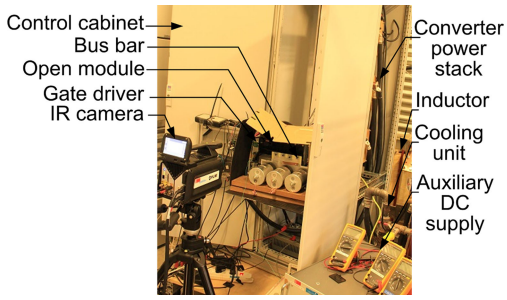

Fig. 17. Test setup featured with IR camera.

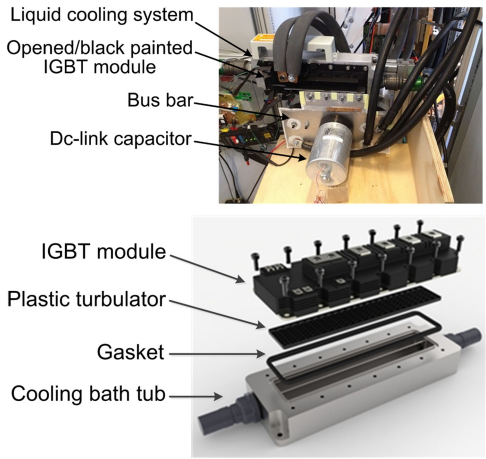

Fig. 18. IGBT module mounted on a cooling system.

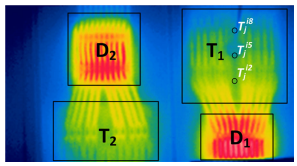

Fig. 19. Thermography of one DCB section at the surface of IGBT module.

P_{loss} = 100 W. As it is clear in Fig. 16, the thermal model is consistent with the FEM simulations. The errors between the thermal model and FEM simulations for all cases are less than 1%.

Furthermore, an experimental setup with the topology shown in Fig. 17 is established to validate the model in a real power cycling operation. The fundamental frequency of the converter is set to 6 Hz, which is usual in reliability power cycling tests [24]. A black painted, opened IGBT module is being monitored by an IR camera (see Fig. 17). The IGBT module is mounted on a direct liquid cooling system, as shown in Fig. 18, where the liquid cooling temperature and the flow rate can be controlled for each experiment and to cool down the IGBT module homogenously [25], [26].

An infrared thermal image of one DCB section of IGBT module is shown in Fig. 19. In order to compare the temperatures monitored by the infrared camera and the temperatures extracted by the thermal model, same monitoring nodes as the 3-D thermal network are considered on the surface of the IGBT/diode chips. As seen in Fig. 19, the nodes are between the bond-wires to monitor the chip surface temperature and not to monitor the bond-wires temperature. Although the experimental verification

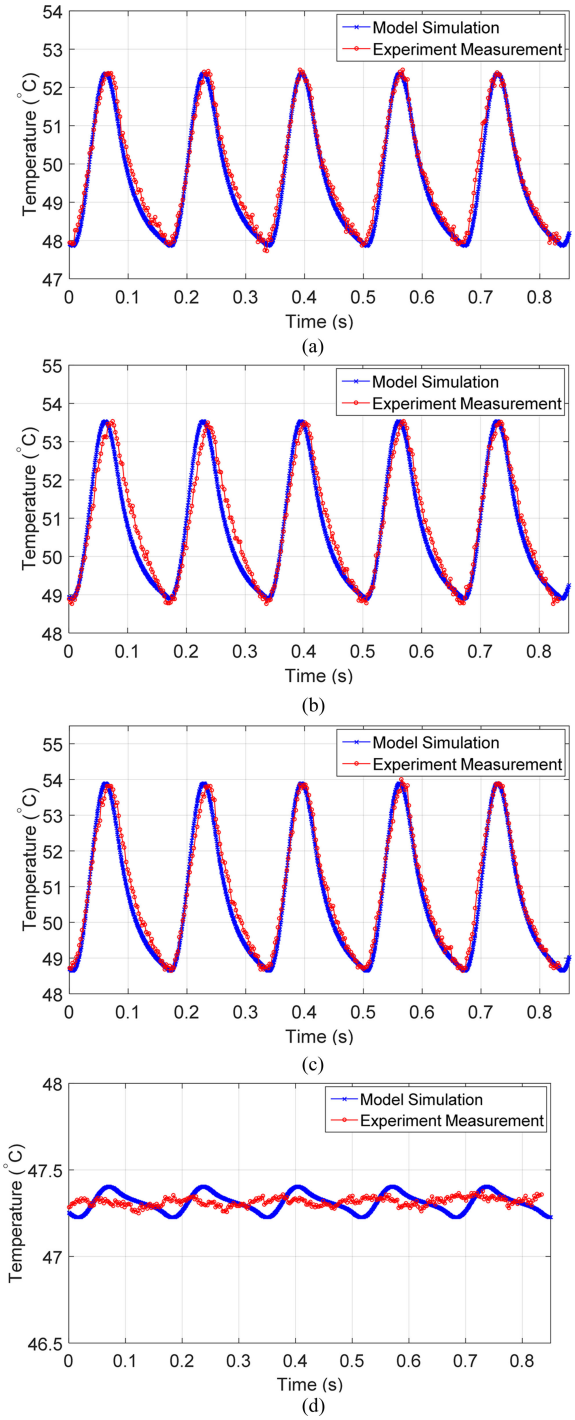

Fig. 20. Junction and case temperatures by thermal model simulation and experimental measurement in $I_{\mathrm{load(peak)}} = 500$ A, $\dot{V} = 5$ m/h, and $T_{\mathrm{cooling}} = 45$ °C: (a) T_2, (b) T_5, (c) T_8, and (d) case.

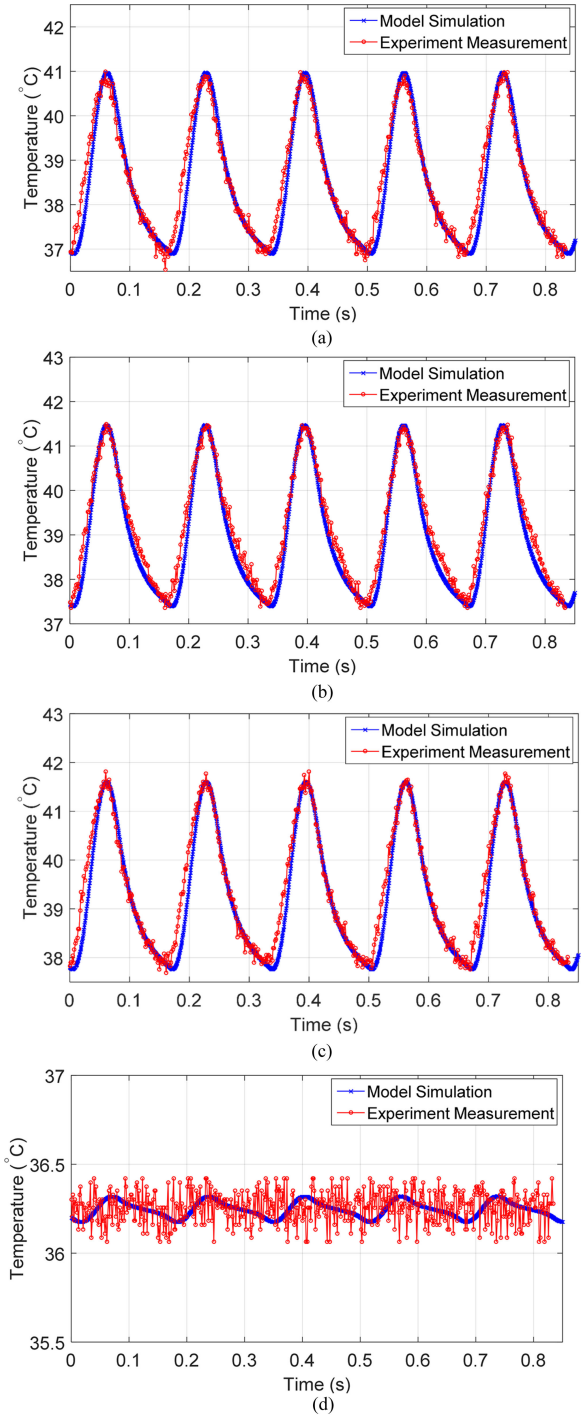

Fig. 21. Junction and case temperatures by thermal model simulation and experimental measurement in $I_{\mathrm{load(peak)}} = 700$ A, $\dot{V} = 1$ m^3/h, and $T_{\mathrm{cooling}} = 34$ °C: (a) T_2, (b) T_5, (c) T_8, and (d) case.

of the internal nodes temperatures is impossible because of inaccessibility of nodes in thermography, accuracy of internal nodes temperatures have been verified by FEM in [20].

Similarly to the experimental setup, a 2L-VSC is established in the circuit simulator—PLECS in this study—and the 3-D thermal impedance network is established. The IGBT/diode chips power losses are identified and injected to the thermal network. To be ensured about the validity of model in different boundary conditions, two scenarios are implemented in the experiments. For the first experiment, the load current is fixed to 500 A (peak), the flow rate of the cooling water is fixed to 5 m^3/h, and the cooling water temperature is fixed to 45 °C. In order to identify the equivalent htc, the water cooling system is simulated in FEM and the htc is extracted in the boundary of the baseplate and coolant. In the first experiment, the equivalent htc is obtained as 7000 W/m^2·K. Because of difficulties in obtaining accurate power losses in the experimental setup, the power losses are calculated by datasheet of the IGBT module and fed to the 3-D

thermal model in order to get the same case temperature with the experiments. Using this method, the power losses are adjusted by $\pm 10\%$ that is a reasonable range in power loss calculations based on the datasheet.

The temperature results for the junction monitoring points T_2, T_5 and T_8 (as it can be seen Fig. 4) and the case obtained by the experiment and simulation are shown in Fig. 20. As it is clear from Fig. 20, the boundary-dependent thermal model gives the temperature with high accuracy—the error is less than 2%. It is worth to mention that the main features in using the boundary-dependent thermal model is the high accuracy in calculation of pick-to-pick temperatures ΔT and the maximum temperature $T_{\max}$ in the junction and internal temperatures. Both ΔT and $T_{\max}$ parameters are critical in lifetime models for the IGBT module, which consider the bond-wire liftoff and solder crack failures [27]. The second experiment is implemented with different boundary conditions: $I_{\mathrm{load(peak)}} = 700$ A, $\dot{V} = 1$ m^3/h (htc $= 3000$ W/m^2·K), and $T_{\mathrm{cooling}} = 34$ °C. As it is shown in Fig. 21, the thermal results are consistent with the experimental results for the both parameters ΔT and $T_{\max}$—with the maximum error of 4%.

VI. Conclusion

In this paper, a simplified boundary-dependent thermal model for high-power IGBT modules has been presented. The boundary conditions, which were applied in the model, are the heat source (power losses) and the heatsink (cooling system). The presented thermal model is a generic *RC* lumped network, which is controlled by changing the heat source and heatsink. It has been proven that varying the power losses influences the junction to chip solder region of IGBT module, because of higher transient thermal impedance variations. Besides, by making changes in the cooling system, the lower layers closer to the heatsink are more affected. By translation of the FEM thermal model, a boundary-dependent 3-D thermal network model for a circuit simulator has been extracted, which can estimate detailed and accurate temperatures of the power module in different locations and layers. The thermal model has been validated by FEM and also by experiments. It has the benefits of FEM accuracy and circuit simulator speed, and it can be used for accurate and detailed temperature estimation in real operating conditions. As the boundary-dependent thermal model can calculate steady-state junction ΔT and $T_{\max}$, the simulated temperature profiles can be used for accurate life-time estimation of the IGBT modules for long-term mission profiles.

Acknowledgment

The authors would like to thank Danfoss Silicon Power GmbH for their support and providing device and cooling system information.

References

[1] S. Yantao and W. Bingsen, "Survey on reliability of power electronic systems," *IEEE Trans. Power Electron.*, vol. 28, no. 1, pp. 591–604, Jan. 2013.

[2] H. Wang, M. Liserre, and F. Blaabjerg, "Toward reliable power electronics: Challenges, design tools, and opportunities," *IEEE Ind. Electron. Mag.*, vol. 7, no. 2, pp. 17–26, Jun. 2013.

[3] A. S. Bahman, F. Iannuzzo, and F. Blaabjerg, "Mission-profile-based stress analysis of bond-wires in SiC power modules," *Microelectron. Reliab.*, vol. 64, p. 419–424, Sep. 2016.

[4] A. S. Bahman, K. Ma, and F. Blaabjerg, "Thermal impedance model of high power IGBT modules considering heat coupling effects," in *Proc. Electron. App. Conf. Expo.*, 2014, pp. 1382–1387.

[5] H. Wang, M. Liserre, F. Blaabjerg, P. de Place Rimmen, J. B. Jacobsen, T. Kvisgaard, and J. Landkildehus, "Transitioning to physics-of-failure as a reliability driver in power electronics," *IEEE J. Emerg. Sel. Topics Power Electron.* vol. 2, no. 1, pp. 97–114, Mar. 2014.

[6] ABB, "Thermal design and temperature ratings of IGBT modules," *App. Note 5SYA 2093-00*, ABB Switzerland Ltd. Semiconductors, Lenzburg, Switzerland, pp. 5–6, 20 Aug. 2013.

[7] D. Cottet, U. Drofenik, and J.-M. Meyer, "A systematic design approach to thermal-electrical power electronics integration," in *Proc. Electron. Syst.-Integr. Technol. Conf.*, 2008, pp. 219–224.

[8] T. Kojima, Y. Yamada, Y. Nishibe, and K. Torii, "Novel RC compact thermal model of HV inverter module for electro-thermal coupling simulation," in *Proc. Power Convers. Conf.*, 2007, pp. 1025–1029.

[9] S. Carubelli and Z. Khatir, "Experimental validation of a thermal modelling method dictated to multichip power modules in operating conditions," *Microelectron. J.*, vol. 34, pp. 1143–1151, Jun. 2003.

[10] V. Szekely, "Identification of RC networks by deconvolution: Chances and limits," *IEEE Trans. Circuits Syst. I, Fundam. Theory Appl.*, vol. 45, no. 3, pp. 244–258, Mar. 1998.

[11] I. R. Swan, A. T. Bryant, N. A. Parker-Allotey, and P. A. Mawby, "3-D thermal simulation of power module packaging," in *Proc. IEEE Energy Convers. Congr. Expo.*, 2009, pp. 1247–1254.

[12] Y. C. Gerstenmaier, A. Castellazzi, and G. K. M. Wachutka, "Electrothermal simulation of multichip-modules with novel transient thermal model and time-dependent boundary conditions," *IEEE Trans. Power Electron.*, vol. 21, no. 1, pp. 45–55, Jan. 2006.

[13] Y. C. Gerstenmaier and G. Wachutka, "Time dependent temperature fields calculated using eigenfunctions and eigenvalues of the heat conduction equation," *Microelectron. J.*, vol. 32, pp. 801–808, 2001.

[14] B. Allard, X. Jorda, P. Bidan, A. Rumeau, H. Morel, X. Perpina, M. Vellvehi, and S. M'Rad, "Reduced-order thermal behavioral model based on diffusive representation," *IEEE Trans. Power Electron.*, vol. 24, no. 12, pp. 2833–2846, Dec. 2009.

[15] H. T. Chen, D. Y. Lin, S. C. Tan, and S. Y. (Ron). Hui, "Chromatic, photometric and thermal modeling of LED systems with non-identical LED devices," *IEEE Trans. Power Electron.*, vol. 29, no. 12, pp. 6636–6647, Dec. 2014.

[16] D. V. Hutton, *Fundamentals of Finite Element Analysis*, Freiburg, Germany: Mcgraw-Hill, 2003.

[17] M. Ibrahim, S. Bhopte, B. Sammakia, B. Murray, M. Iyengar, and R. Schmidt, "Effect of transient boundary conditions and detailed thermal modeling of data center rooms," *IEEE Trans. Compon. Packag. Manuf. Technol.*, vol. 2, no. 2, pp. 300–310, Feb. 2012.

[18] J. H. Lienhard, IV, and J. H. Lienhard, V, *A Heat Transfer Textbook*, 3rd *ed*. Cambridge, MA, USA: Phlogiston Press, 2006.

[19] ANSYS® Academic Research, Icepak Release 16.1, 2015.

[20] A. S. Bahman, K. Ma, P. Ghimire, F. Iannuzzo, and F. Blaabjerg, "A 3D lumped thermal network model for long-term load profiles analysis in high power IGBT modules," *IEEE J. Emerg. Sel. Topics Power Electron.*, vol. 4, no. 3, pp. 1050–1063, Sep. 2016.

[21] N. Y. A. Shammas, "Present problems of power module packaging technology," *Microelectron. Rel.*, vol. 43, pp. 519–527, Apr. 2003.

[22] M. Musallam and C. M. Johnson, "Real-time compact thermal models for health management of power electronics," *IEEE Trans. Power Electron.*, vol. 25, no. 6, pp. 1416–1425, Jun. 2010.

[23] MATLAB version 8.1.0.604, The MathWorks Inc., Natick, MA, USA, 2013.

[24] P. Ghimire, A. R. de Vega, S. Beczkowski, B. Rannestad, S. M. -Nielsen, and P. Thogersen, "Improving power converter reliability: Online monitoring of high-power IGBT modules," *IEEE Ind. Electron. Mag.*, vol. 8, no. 3, pp. 40–50, Sep. 2014.

[25] K. Olesen, R. Bredtmann, and R. Eisele, "ShowerPower® new cooling concept," in *Proc. PCIM'2004*, 2004, pp. 1–9.

[26] A. S. Bahman and F. Blaabjerg, "Optimization tool for direct water cooling system of high power IGBT modules," in *Proc. 2016 European Conf. Power Electron. Appl.*, 2016, pp. 1–10.

[27] A. S. Bahman, K. Ma, and F. Blaabjerg, "General 3D lumped thermal model with various boundary conditions for high power IGBT modules," in *Proc. Appl. Power Electron. Conf. Expo.*, 2016, pp. 261–268.

Amir Sajjad Bahman (S'08–M'15) received the B.Sc. degree from Iran University of Science and Technology, Tehran, in 2008, the M.Sc. degree from Chalmers University of Technology, Göteborg, Sweden, in 2011, and the Ph.D. degree from Aalborg University, Aalborg, Denmark, in 2015, all in electrical engineering.

He was a Visiting Scholar with the Department of Electrical Engineering, University of Arkansas, USA, in 2014. He was the Thermal Design Engineer with Danfoss Silicon Power, Germany, in 2014, and the Electrical Design Engineer with Aryacell Telecommunication Company, Iran, from 2011 to 2012. He is currently a Postdoctoral Fellow at the Center of Reliable Power Electronics (CORPE), Aalborg University. His current research interests include electrothermomechanical modeling, packaging, and reliability of power electronic systems and components.

Ke Ma (S'09–M'11) received the B.Sc. and M.Sc. degrees in electrical engineering from the Zhejiang University, Zhejiang, China, in 2007 and 2010, respectively, and the Ph.D. degree from Aalborg University, Aalborg, Denmark, in 2013.

In 2013, he was a Postdoctoral Fellow with Aalborg University and became an Assistant Professor in 2014. He was with Vestas Wind Systems A/S, Denmark, in 2015. In 2016, he joined the faculty of Shanghai Jiao Tong University, Shanghai, China, as a Tenure-Track Research Professor. His current research interests include the design and enhancement of power electronics reliability in the application of renewable energy and motor drive systems.

Dr. Ma is the Associate Editor for the IEEE TRANSACTIONS ON INDUSTRY APPLICATIONS and Guest Associate Editor for the IEEE JOURNAL OF EMERGING AND SELECTED TOPICS IN POWER ELECTRONICS. In 2016, he was awarded with the "Thousand Talents Plan Program for Young Professionals" of China. He was the receiver of "Excellent Young Wind Doctor Award 2014" by European Academy of Wind Energy, and several prize paper awards by the IEEE.

Frede Blaabjerg (S'86–M'88–SM'97–F'03) received the Ph.D. degree in electrical engineering from Aalborg University, Aalborg, Denmark in 1995.

He was with ABB-Scandia, Randers, Denmark, from 1987 to 1988. He became an Assistant Professor in 1992, Associate Professor in 1996, and Full Professor of Power Electronics and Drives in 1998 at Aalborg University. His current research interests include power electronics and its applications such as in wind turbines, photovoltaic (PV) systems, reliability engineering, power quality, and adjustable speed drives.

Dr. Blaabjerg has received 18 IEEE Prize Paper Awards, the IEEE PELS Distinguished Service Award in 2009, the EPE-PEMC Council Award in 2010, the IEEE William E. Newell Power Electronics Award 2014, and the Villum Kann Rasmussen Research Award 2014. He was an Editor-in-Chief of the IEEE TRANSACTIONS ON POWER ELECTRONICS from 2006 to 2012. He was nominated in 2014, 2015, and 2016 by Thomson Reuters to be between the most 250 cited researchers in engineering in the world. In 2017, he became Doctor Honoris Causa at the University of Politehnica in Timisoara, Romania.